Materials Science & Engineering C 92 (2018) 590–598

Contents lists available at ScienceDirect

Materials Science & Engineering C

journal homepage: www.elsevier.com/locate/msec

Non-enzymatic electrochemical hydrogen peroxide biosensor based on reduction graphene oxide-persimmon tannin-platinum nanocomposite

Yong Huang[a,b,1], Yewei Xue[a,1], Junxiang Zeng[a], Shanshan Li[a], Zhihong Wang[a], Chenyang Dong[a], Guiyin Li[a,b,*], Jintao Liang[a,**], Zhide Zhou[a,**]

[a] School of Life and Environmental Sciences, Guilin University of Electronic Technology, Guilin, Guangxi 541004, China
[b] National Center for International Research of Biological Targeting Diagnosis and Therapy, Guangxi Key Laboratory of Biological Targeting Diagnosis and Therapy Research, Collaborative Innovation Center for Targeting Tumor Diagnosis and Therapy, Guangxi Medical University, Nanning, Guangxi 530021, China

ARTICLE INFO

Keywords:
Hydrogen peroxide
Reduction graphene oxide
Persimmon tannin
Pt nanoparticles
Non-enzymatic biosensor

ABSTRACT

Hydrogen peroxide (H_2O_2) is one of the most universal and essential ingredients in distinct biological tissues. Herein, a novel non-enzymatic sensor based on reduction graphene oxide-persimmon tannin-platinum nanocomposite (RGO-PT-Pt) was exploited for H_2O_2 detection. RGO-PT-Pt nanocomposite was prepared by reduction procedure with ascorbic acid as reducing agent and characterized by Scanning electron microscopy (SEM), Transmission electron microscopy (TEM), ultraviolet visible spectroscopy (UV–vis) and Fourier infrared spectroscopy (FT-IR). Taking advantage of high electro-catalytic efficiency of Pt nanoparticles, high electronic conductivity and large surface area of RGO, and significant adsorption ability of PT on metal ions and its prevention of agglomeration to promote RGO dispersion, RGO-PT-Pt nanocomposite revealed better catalytic ability towards H_2O_2 via a synergistic effect. Under the optimal conditions, the RGO-PT-Pt non-enzymatic biosensor exhibited outstanding electrocatalytic activity towards H_2O_2 reduction. The amperometric response demonstrated a linear relationship with H_2O_2 concentration from 1.0 to100 μM with the correlation coefficient of 0.9931. The limit of detection was 0.26 μM (S/N = 3) and the response time was 3 s. Furthermore, the fabricated sensor exhibited a practical applicability in the quantification of H_2O_2 in human serum samples with an excellent recovery rate. Due to excellent performance such as fast response time, low detection limit, high stability and selectivity, the RGO-PT-Pt non-enzymatic biosensor has potential application in clinical diagnostics.

1. Introduction

Hydrogen peroxide (H_2O_2) is one of the most universal and essential ingredients in distinct biological tissues [1]. In the case of depletion of antioxidants, the oxidation of biomolecules can cause oxidative stress leading to elevated levels of H_2O_2 and other reactive oxygen species, which in turn leads to neurological disorders, autoimmune diseases, and even cancer [2]. The concentration of H_2O_2 is rather low under normal physiological and can increase to $\sim 10^{-3}$ M under pathological conditions such as traumatic brain injury, ischemia-reperfusion, environmental stresses, and so on [3]. H_2O_2 plays an important role as a signal constituent to regulate miscellaneous biological processes [4–6]. Consequently, there is an increasing demand for fast, reusable, high sensitivity and cost-effective analytical methods for H_2O_2 detection.

To date, many methods have been used for the H_2O_2 detection, such as titration [7], spectrofluorometry [5, 8], chemiluminescence [9], photocolorimetry [10], electrochemical analysis and so on [11–13]. Among them, electrochemical techniques, especially enzyme-based electrochemical sensors, are particularly favored with high efficiency, significant selectivity and activity [14–16]. However, natural enzymes are sensitive to the environmental conditions and the instability of enzyme-based biosensors is inevitable. Therefore, non-enzymatic biosensors have aroused great attention because of their simplicity, low cost, high reliability and sensitivity [6, 17]. For instance, Thanh et al. [18] have constructed an effective non-enzymatic sensor based on porous gold-palladium nanoalloy network-supported graphene nanohybrids (Au Pd@GR) with excellent catalytic activity towards H_2O_2 detection. Although a great deal of non-enzymatic H_2O_2 sensor have been designed, the study of nanomaterials with higher catalytic activity towards H_2O_2 detection is still a great challenge [19].

* Correspondence to: G.Y. Li, School of Life and Environmental Sciences, Guilin University of Electronic Technology, Guilin, Guangxi 541004, China.
** Corresponding authors.
E-mail addresses: liguiyin01@163.com (G. Li), dxljt@163.com (J. Liang), zzdlgy@163.com (Z. Zhou).
[1] These authors contributed equally to this work.

https://doi.org/10.1016/j.msec.2018.07.021
Received 31 October 2017; Received in revised form 30 June 2018; Accepted 8 July 2018
Available online 11 July 2018
0928-4931/

RGO has excellent electrical and mechanical properties because of the loss of oxygen-containing functional groups which made it stable compared to GO [13, 20, 21]. RGO provides a number of active defect sites with significant turbulence and enlarge layer spacing that can effectively trap active species [2, 22, 23]. Moreover, RGO is an excellent carrier to assist other nanoparticles to obtain rapid electrochemical kinetics during electro-catalytic reactions, resulting in faster and more sensitive current response. However, due to the strong π-π stacking among the molecular, RGO would easily generate the reunion and interlayer, which will affect the dispersion and hinder the further applications [24, 25]. Therefore, it is necessary to enhance the dispersibility of RGO in solution with the appropriate biopolymer.

Persimmon tannin (PT), produced from the persimmon extract, is an eco-friendly, water-soluble and low-cost natural biopolymer with multiple adjacent phenolic hydroxyl groups [26, 27]. PT shows high affinity towards Au, Pt, Pd and other metal ions by chelating reaction, thus the effective adsorption of metal ions [28–30]. PT is able to adsorb onto the surface of graphene by π-π and electrostatic interactions to prevent RGO agglomeration, and the mixed material would prove better tenability of particle size, shape and high specific surface area for loading more guest molecules [28, 31].

It is well known that noble metal nanoparticles exhibit outstanding electro-catalytic activity towards H_2O_2 redox reactions [32–35]. Among them, Pt nanoparticles (Pt NPs) are used as an excellent electro-catalyst for the detection of H_2O_2 because Pt NPs can trigger a strong electrocatalytic current for the evolution of H_2O_2 and lower the H_2O_2 oxidation/reduction overvoltage efficiently [36].

In this work, a facile and effective non-enzymatic H_2O_2 biosensor was constructed based on RGO-PT-Pt nanocomposite. The RGO-PT-Pt nanocomposite was synthesized through a facile approach with ascorbic acid (AA) as reducing agent. PT acts as an appropriate biopolymer to prevent RGO agglomeration and enhance the dispersibility of RGO. The conformation of the RGO-PT-Pt nanocomposite was characterized by SEM, TEM, UV–vis and FT-IR. Taking advantage of the high electro-catalytic efficiency of Pt NPs, high electronic conductivity and high surface area of RGO, and the excellent adsorption capacity of PT on metal ions and its prevention of agglomeration to promote RGO dispersion, the RGO-PT-Pt nanocomposite revealed better catalytic ability to H_2O_2 via synergistic effect. This novel non-enzymatic H_2O_2 biosensor exhibited excellent electrocatalytic performance towards H_2O_2 such as fast amperometric response time, low detection limit, high stability and selectivity.

2. Materials and methods

2.1. Chemicals and reagents

Sample of dry persimmon tannin powder (the feed material extracted from astringent persimmon) was amicable donated by Guangxi Dekun Company of Agricultural Products (Guangxi, China). Graphene oxide (GO) was purchased from TIMENANO Company (Chengdu, China). $HAuCl_4$ and $H_2PtCl_6{\cdot}6H_2O$ were obtained from Guangfu Fine Chemical Co., Ltd. (Tianjin, China). Ascorbic acid (AA), uric acid (UA), hydrochloride (DA) and dihydroxy phenyl acetic acid (DOPAC) were purchased from Shanghai Linc-Bio Science Co., Ltd. (Shanghai, China). All other reagents were of analytical grade and used without any further purification. All the solutions were prepared with ultrapure water of 18 MΩ purified from a Milli-Q purification system (Milli-Pore, Bedford, MA, USA). The human blood serum was acquired from 181st Hospital of Chinese People's Liberation Army (Guilin, China).

2.2. Apparatus

The morphology and structure of the RGO-PT-Pt nanocomposite were characterized by scanning electron microscopy (SEM, Quanta 200, Elementar, Germany) and Transmission electron microscopy (TEM, JEM-2100F, Japan), Fourier transform infrared spectroscopy (FT-IR, Bruker Tensor 27, Germany), ultraviolet visible spectroscopy (UV–vis, UH5300, HITACHI, Japan), Raman microscope (RM, Thermo DXRxi, Renishaw, UK) and X-ray photoelectron spectroscopy (XPS, ESCALAB 250Xi, Thermo Fisher, USA).

All electrochemical measurements were performed on CHI660D electrochemical workstation (Shanghai Chenhua Instrument, China) at room temperature. A conventional screen-printed carbon electrode (SPCE, Nanjing Yunyou Biotech Co., Ltd., China) system was used for all electrochemical measurements: one carbon paste electrode or modified carbon paste electrode as the working electrode, another carbon paste electrode as the auxiliary electrode and Ag/AgCl electrode as the reference electrode. Cyclic voltammetry (CV) was performed in phosphate buffer saline (PBS, pH 7.4, 0.1 M Na_2HPO_4/KH_2PO_4 and 0.1 M NaCl) containing 5 mM $K_3Fe(CN)_6/K_4Fe(CN)_6$ and 0.1 M KCl with scanning range from −0.3 to 0.6 V and scanning rate of 100 mV/s. Electrochemical impedance spectroscopy (EIS) was acquired in PBS containing 5 mM $K_3Fe(CN)_6/K_4Fe(CN)_6$ and 0.1 M KCl at +0.24 V from 0.1 Hz to 100 KHz. The amperometric curve technique (i-t) was carried out in PBS under the constantly stirring.

2.3. Preparation of the RGO-PT-Pt nanocomposite

RGO-PT-Pt nanocomposite was synthesized through a facile approach with AA as reducing agent. Firstly, 10 mL 0.1 mg/mL of GO was dispersed with ultrasonic for 2 h to form a uniform suspension, then 10 mg AA was slowly added and stirred for 12 h. Following that, the mixed solution was centrifuged for 15 min at 10,000 rpm, removed the supernatant, washed twice with ultrapure water and got the RGO. Secondly, 20 mg PT was added into 10 mL 0.1 mg/mL RGO dispersion and ultrasonic dispersed uniformly for 30 min to gain well-distributed RGO-PT suspension. Thirdly, 4 mL 1% H_2PtCl_6 solution and 10 mg AA were added into the RGO-PT suspension and stirred for 20 h. Fourthly, the above mixed solution was centrifuged at 10,000 rpm for 15 min, removed the supernatant and washed three times with ultrapure water. Lastly, the precipitates were re-dispersed in ultrapure water to form 1.0 mg/mL RGO-PT-Pt nanocomposite suspension and stored in refrigerator at 4 °C before use.

2.4. Preparation of the non-enzymatic electrochemical biosensor based on RGO-PT-Pt nanocomposite

The bare SPCE was first activated by placing in a 0.5 M H_2SO_4 solution and scanning by CV for 10 cycles with the scanning voltage range from −0.2 to 1.0 V and the scanning rate of 100 mV/s. Then, Au NPs was deposited onto the activated SPCE in 5 mL of 0.01% $HAuCl_4$ solution at room temperature under a constant potential of −0.5 V for 120 s while the magnetic stirring. After the Au NPs/SPCE was cleaned with ultrapure water and dried, 18 μL of RGO-PT-Pt nanocomposite dispersion was added dropwise onto the surface of Au NPs/SPCE and incubated at 26 °C for 30 min. Then the working electrode was cleaned again with ultrapure water to obtain the RGO-PT-Pt/Au NPs/SPCE and stored in refrigerator at 4 °C before use. Thus, a non-enzymatic electrochemical biosensor based on the RGO-PT-Pt nanocomposites (RGO-PT-Pt biosensor) was fabricated.

2.5. Electrochemical detection of H_2O_2 with RGO-PT-Pt non-enzymatic biosensor

The detection of H_2O_2 was performed by i-t at a voltage of −0.4 V with RGO-PT-Pt/Au NPs/SPCE as the working electrode and PBS as the supporting electrolyte. During the measurement, 10 μL H_2O_2 was continuously added to 10 mL of PBS solution and record the electrochemical signals generated by different concentrations of H_2O_2.

2.6. Exploration of the anti-interference capability of RGO-PT-Pt non-enzymatic biosensor

In order to explore the anti-interference performance of RGO-PT-Pt non-enzymatic biosensor, AA, UA, DA and DOPAC were selected as interfering substances experiment. The amperometric responses were recorded with the successive addition of 0.1 mM H_2O_2, 0.1 mM AA, 0.1 mM UA, 0.1 mM DA, 0.1 mM DOPAC and a second 0.1 mM H_2O_2 into 10 mL PBS at a voltage of −0.4 V.

2.7. Application in human serum samples of the RGO-PT-Pt non-enzymatic biosensor

To demonstrate the possible application of the proposed method, human serum samples were assayed using the standard addition method by the RGO-PT-Pt non-enzymatic biosensor. Human serum samples were donated by local hospitals. A known quantitative H_2O_2 solution (15 μM, 40 μM, 60 μM) was added dropwise to a solution of 10 mL 0.1 M PBS containing 200 μL human serum. The level of H_2O_2 in the spiked sample was measured in parallel 3 times with i-t using the developed H_2O_2 biosensor.

3. Results and discussion

3.1. Analytical principle of RGO-PT-Pt non-enzymatic biosensor for detection of H_2O_2

Herein, a novel non-enzymatic biosensor for H_2O_2 detection was constructed based on RGO-PT-Pt nanocomposite, and the analytical principle was schematically described in Fig.1A. First, RGO-PT-Pt nanocomposite was successfully prepared through a facile approach with AA as reducing agent. Then, the bare SPCE was activated by H_2SO_4, and electrodeposited of Au NPs onto the surface of SPCE through the isostatic potentiometric deposition, which will increase the effective area of the work electrode. After that, the RGO-PT-Pt nanocomposite was immobilized onto the surface of the Au NPs/SPCE due to the π-π and electrostatic adsorption. Thus a non-enzymatic electrochemical H_2O_2 biosensor, RGO-PT-Pt non-enzymatic biosensor, was fabricated. The detection of H_2O_2 was performed by i-t at a voltage of −0.4 V with RGO-PT-Pt/Au NPs/SPCE as the working electrode and PBS as the supporting electrolyte. The amperometric responses were recorded with the successive addition of H_2O_2. The current response was directly proportional to the concentration of H_2O_2 so that the H_2O_2 was detected with high sensitivity.

Among the RGO-PT-Pt nanocomposite, RGO was used not only to increase the electrical conductivity of the bio-composite film but also to provide specific surface area. PT acted as an appropriate biopolymer to prevent RGO agglomeration and enhance the dispersibility of RGO. At the same time, PT acted as bio-composite film material to adsorb metal ions (Pt^{4+}), the latter was then reduced to Pt NPs by AA, and Pt NPs have the excellent catalytic ability for disintegration of the H_2O_2 and electron conductivity. All in all, the integration of different ingredients in the RGO-PT-Pt nanocomposite displayed their merits of each component, and exhibited excellent catalytic ability to H_2O_2 via a synergistic effect.

Fig. 1B depicted the amperometric response of the developed RGO-PT-Pt non-enzymatic biosensor for H_2O_2 detection at a voltage of −0.4 V using the amperometric i-t technique. As can be seen in Fig. 1B, there was a remarkable ladder-like current response ($\Delta I = 356 \pm 49.5$ nA) in the presence of H_2O_2 (curve b). As a control, an unconspicuous response appeared under the absence of H_2O_2 (curve a).

In addition, Fig. 1C showed the current response for the measurement of H_2O_2 by non-enzymatic sensors with different materials, where the curves a, b, c, d and e represented the bare SPCE, Au NPs/SPCE, RGO/Au NPs/SPCE, RGO-PT/Au NPs/SPCE, RGO-PT-Pt/Au NPs/SPCE, respectively. It was evident that RGO-PT-Pt/Au NPs/SPCE exhibited the highest amperometric response for H_2O_2 detection (curve e) compared with the other different materials.

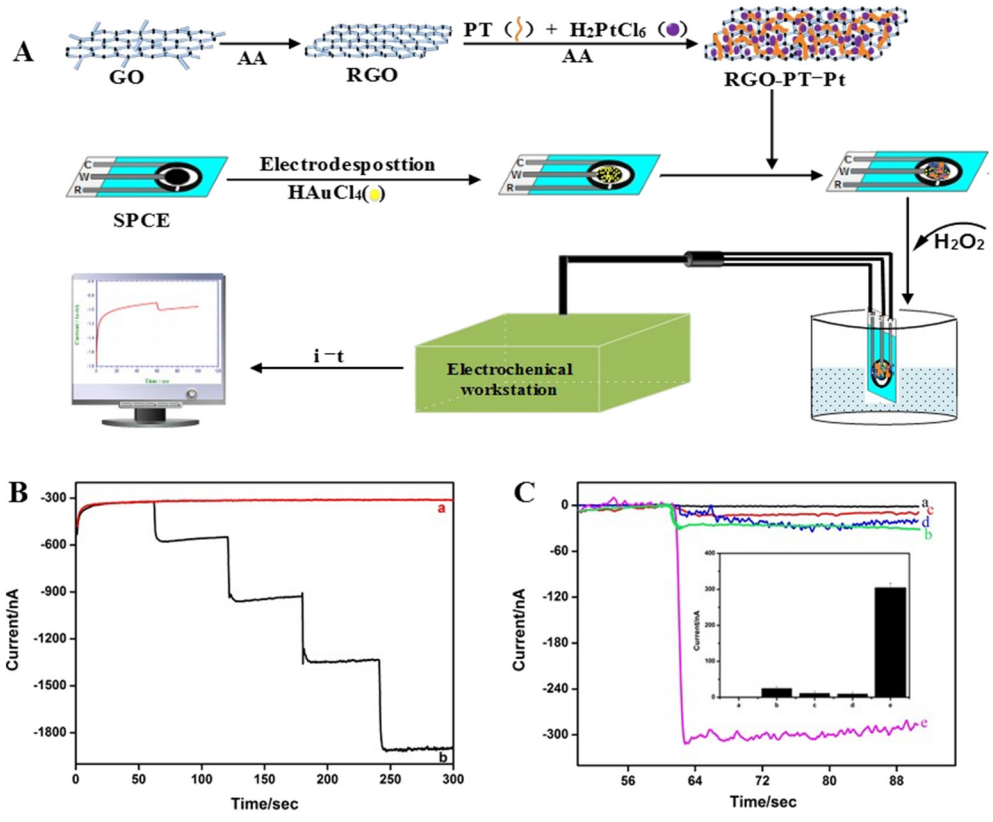

Fig. 1. (A) Principle of non-enzymatic biosensor based on RGO-PT-Pt composites for detection H_2O_2; (B) Current-time curve of the non-enzymatic biosensor (a) without and (b) with 0.1 mM H_2O_2 at a voltage of −0.4 V; (C) The current response curves of H_2O_2 were detected by non-enzymatic biosensors of different materials: SPCE (a), Au NPs/SPCE (b),RGO/Au NPs/SPCE (c), RGO-PT/Au NPs/SPCE (d),RGO-PT-Pt/Au NPs/SPCE (e),Illustration was the histogram of the corresponding response current.

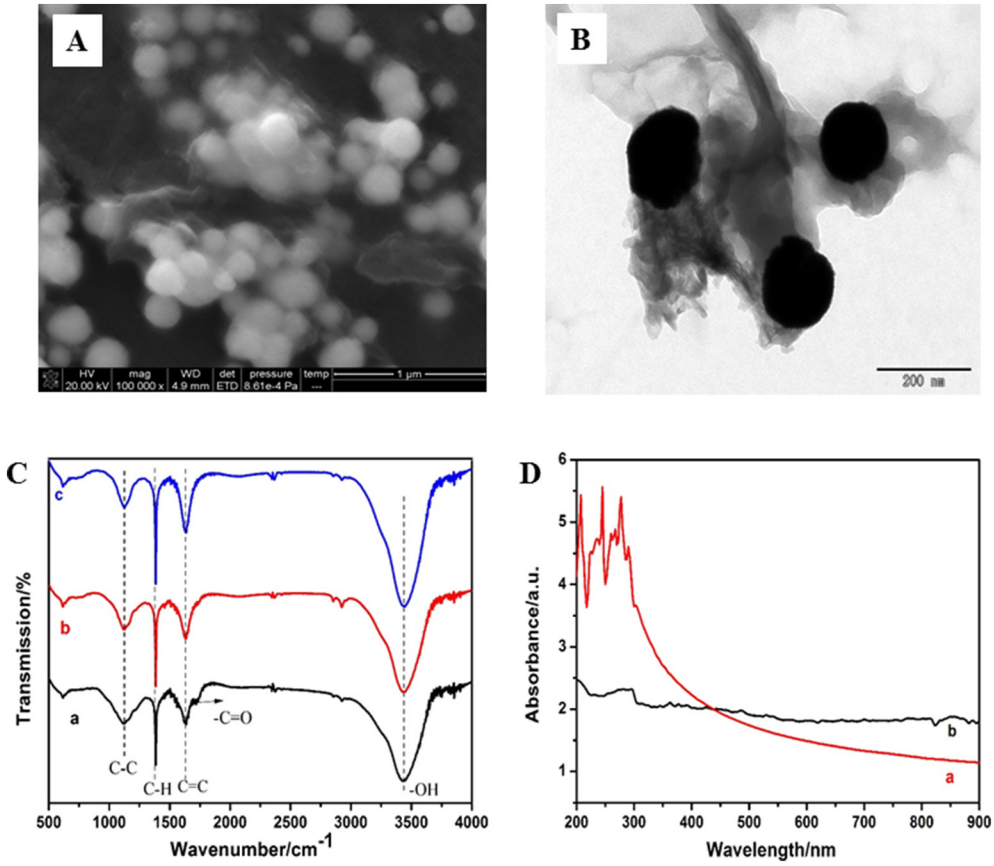

Fig. 2. (A) SEM image for RGO-PT-Pt nanocomposite; (B) TEM image for RGO-PT-Pt nanocomposite; (C) FT-IR spectra of GO (a), RGO (b), RGO-PT-Pt nanocomposite (c); (D) UV–vis spectra of RGO (a), and RGO-PT-Pt nanocomposite (b).

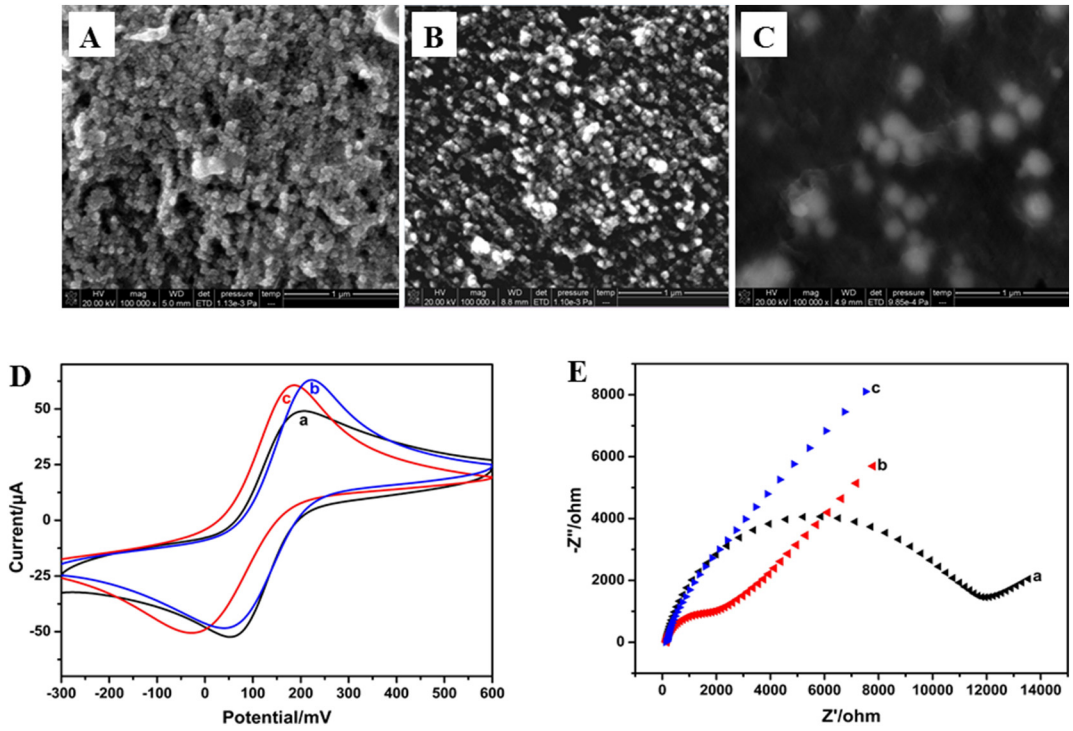

Fig. 3. SEM images for bare SPCE (A); Au NPs/SPCE (B); RGO-PT-Pt/Au NPs/SPCE (C); (D) Cyclic voltammetry response for bare SPCE (a), Au NPs/SPCE (b), RGO-PT-Pt/Au NPs/SPCE (c) in PBS containing 5 mM $K_3Fe(CN)_6/K_4Fe(CN)_6$ and 0.1 M KCl with scanning range from −0.3 to 0.6 V and scanning rate of 100 mV/s; (E) Electrochemical impedance spectroscopy of bare SPCE (a), Au NPs/SPCE (b), and RGO-PT-Pt/Au NPs/SPCE (c) in PBS containing 5 mM $K_3Fe(CN)_6/K_4Fe(CN)_6$ and 0.1 M KCl at 0.24 V with a frequency range of 0.1–100 kHz.

3.2. Characterization of the RGO-PT-Pt nanocomposites

The typical SEM images of RGO-PT-Pt nanocomposites were shown in Fig. 2A. The image of RGO-PT-Pt nanocomposites (Fig. 2A) showed a uniform distribution of white spherical particles with about 200 ± 10 nm (Pt NPs) on the surface and a layer of film. The spherical particles were Pt NPs and the film may be PT. This implied that the Pt NPs had been successfully generated with a facile approach by AA reduction.

The morphology of RGO-PT-Pt nanocomposites was also studied by TEM. Fig. 2B showed some black spherical particles with the particle size of about 200 nm attached to the top of the membrane. The film would be the mixture of RGO-PT and the black spheres was Pt NPs. This phenomenon was consistent with the SEM analysis.

FT-IR spectrometry is used to characterize the functional groups of the nanomaterials. Fig. 2C described the FT-IR spectra of GO (curve a), RGO (curve b), RGO-PT-Pt (curve c) nanocomposite. The strong and broad band at 3423 cm^{-1} for various samples was assigned to the stretching vibration of the hydroxyl groups. For the GO (Fig. 2C, curve a), the characteristic peaks were found at 1122 cm^{-1} (C—C stretching vibration), 1384 cm^{-1} (C—H stretching vibration), 1637 cm^{-1} (C═C stretching vibration) and 1718 cm^{-1} (C═O stretching vibration), respectively. Compared to the spectrum of GO, the specific peaks in the spectrum of RGO (Fig. 2C, curve b), RGO-PT-Pt (Fig. 2C, curve c) were obviously less and weaker. Specially, the C═O absorption peak had disappeared, which indicated that the GO was reduced to RGO and the RGO-PT-Pt nanocomposite was successfully prepared.

In addition, the UV–vis spectra of RGO (curve a) and RGO-PT-Pt (curve b) nanocomposite were shown in Fig. 2D. There was a significant difference, where RGO had an absorption peak at 245 nm, 277.5 nm and 290 nm, while RGO-PT-Pt had a maximum absorption peak at 295 nm.

3.3. SEM characterization of RGO-PT-Pt non-enzymatic biosensor

Fig. 3A-3C showed the SEM images of the different SPCE modified with various materials. Fig. 3A represented the surface of the bare SPCE, which can be seen that the electrode surface was uneven without particle distribution. Fig. 3B was the surface of the SPCE after the electrodeposition of Au NPs. It can be seen that the bright white particles with uniform distribution on the electrode surface, which showed that the Au NPs had been successfully modified on the electrode surface by electrodeposition. Fig.3C depicted the RGO-PT-Pt nanocomposite fixed on the electrode surface. Compared with that of Fig.3B, the surface of the electrode became smooth, a sheet-like film in which some bright spots randomly distributed in the image of the RGO-PT-Pt nanocomposites modified SPCE.

3.4. Electrochemical behavior of the RGO-PT-Pt non-enzymatic biosensor

Cyclic voltammetry (CV) was used to observe the changes of electrochemical behavior at different stages of the RGO-PT-Pt non-enzymatic biosensor. The CV behavior of the different modification stages of the SPCE was carried out in PBS containing 5 mM $K_4Fe(CN)_6/K_3Fe(CN)_6$ and 0.1 M KCl, and the results were shown in Fig. 3D. Seen from Fig. 3D, a reversible redox peak appeared (49.08 μA) with bare SPCE due to the equivalent amount of $Fe(CN)_6^{4-}$ and $Fe(CN)_6^{3-}$ ions in the reaction medium (Fig. 3D, curve a). Compared to the bare SPCE, the redox peak for the Au NPs/SPCE (Fig. 3D, curve b) increased significantly (62.99 μA). This may be that the Au NPs on the surface of the SPCE facilitates the transfer of electrons. Moreover, an oxidation peak current of 60.65 μA appeared in the RGO-PT-Pt/Au NPs/SPCE (Fig. 3D, curve c), which was relatively larger than the current of bare SPCE, but was less than that of Au NPs/SPCE. This was because that the RGO and Pt NPs in RGO-PT-Pt nanocomposites (curve c) had the effect of increasing the electro-conductivity, but PT was a kind of the polymer materials with weak electro-conductivity.

Furthermore, the average value of the electroactive surface area could be calculated according to the Randles-Sevcik equation [36,[37]]:

$$Ip = 2.69 \times 10^5 AD^{1/2}n^{3/2}\gamma^{1/2}C \quad (1)$$

where Ip means the current peak, A is on behalf of the electroactive surface area (cm^2), D is the diffusion coefficient in the $[Fe(CN)_6]^{3-/4-}$ ($6.70 \pm 0.02 \times 10^{-6}$ cm^2/s), n is the number of electrons participating in the redox reaction (for $[Fe(CN)_6]^{3-/4-}$, $n = 1$), γ represents the scanning rate (V/s) and C delegates the concentration of the redox probe (mol/cm^3).

By calculation, the effective surface area of the working electrode was bare SPCE (0.0446 cm^2) < RGO-PT-Pt/Au NPs/SPCE (0.0551 cm^2) < Au NPs/SPCE (0.0573 cm^2). Therefore, the deposition of Au NPs was beneficial to increase the surface area of the electrode.

Electrochemical impedance spectroscopy (EIS), a valid method for exploring the properties of surface modified electrodes, was performed for the different modification stages of at +0.24 V in PBS containing 5 mM $[Fe(CN)_6]^{3-/4-}$ and 0.1 M KCl, and the results were shown in Fig. 3E. Seen from Fig. 3E, the impedance of the bare SPCE was relatively high with the value of 11,950 Ω (curve a). After deposition of Au NPs on the surface of SPCE (curve b), the resistance was decreased to 1942 Ω because that the presence of Au NPs enhanced the electron transfer rate. When the RGO-PT-Pt nanocomposite was modified to the electrode, the impedance value increased to 2187 Ω (curve c), which indicating that the electron-transfer capacity of the composite material was weaker than the Au NPs. The EIS results were in good agreement with those obtained from CV, revealing the successful fabrication of the RGO-PT-Pt non-enzymatic biosensor.

3.5. XPS characterization of RGO-PT-Pt non-enzymatic biosensor

XPS was further used to estimate effective information on the process for the different stages of SPCE modification. Fig. 4A illustrated the full XPS spectra of all the elements of the modification process of SPCE. Seen from Fig. 4A, a higher intensity C1s (283.05 eV), O1s (531.37 eV) associated with lower intensity peak series of N1 s (398.45 eV), Au4f (82.71 eV). In addition, the appearance of the new Pt 4f (71.08 eV) was related to lower intensity peak series of N1s (398.45 eV), Au4f (82.71 eV).

Fig. 4B showed the XPS characterization of four elements (O1s, N1s, C1s, Au4f) at different stages of SPCE modification. Compared to the bare SPCE (Fig. 4B, curve a), the signals of C1s (283.27 eV), N1s (398.45 eV) and O1s (531.37 eV) decreased, and the Au4f (82.71 eV) signal appeared (Fig. 4B, curve b), which was due to the electrodeposition of Au NPs on the surface of SPCE. However, when the RGO-PT-Pt nanocomposite was immobilized to the Au NPs/SPCE (Fig. 4B, curve c), the signal intensity of O1s (532.04 eV)rapidly increased while the signal intensity C1s (284.45 eV), N1 s (398.97 eV), Au4f (82.90 eV) were relatively weaken with the presence of Pt 4f (71.08 eV) signal due to the adding Pt NPs within the RGO-PT-Pt nanocomposite. The rapidly increased in the O1s was due to the fact that the PT contains a large amount of oxygen, while the C1s was only slightly reduced because of the increase of oxygen leading to decrease of C atom content in the whole system.

Furthermore, the relative abundance (% of atoms) of the various elements (C, O, N, Au, Pt) for reaction processes are summarized in the Table inset Fig. 4A. The immobilized RGO-PT-Pt nanocomposite on the surface of electrode caused a strong increase in the proportion of O from 16.56% to 29.86% and mild decrease in the proportion of C from 75.38% to 68.01%. In addition, the new proportion of Pt was 1.15%, while the proportion of Au decreased strongly from 4.44% to 0.16%.

3.6. Raman spectroscopy of RGO-PT-Pt non-enzymatic biosensor

Raman spectroscopy is a ubiquitously practiced technique for

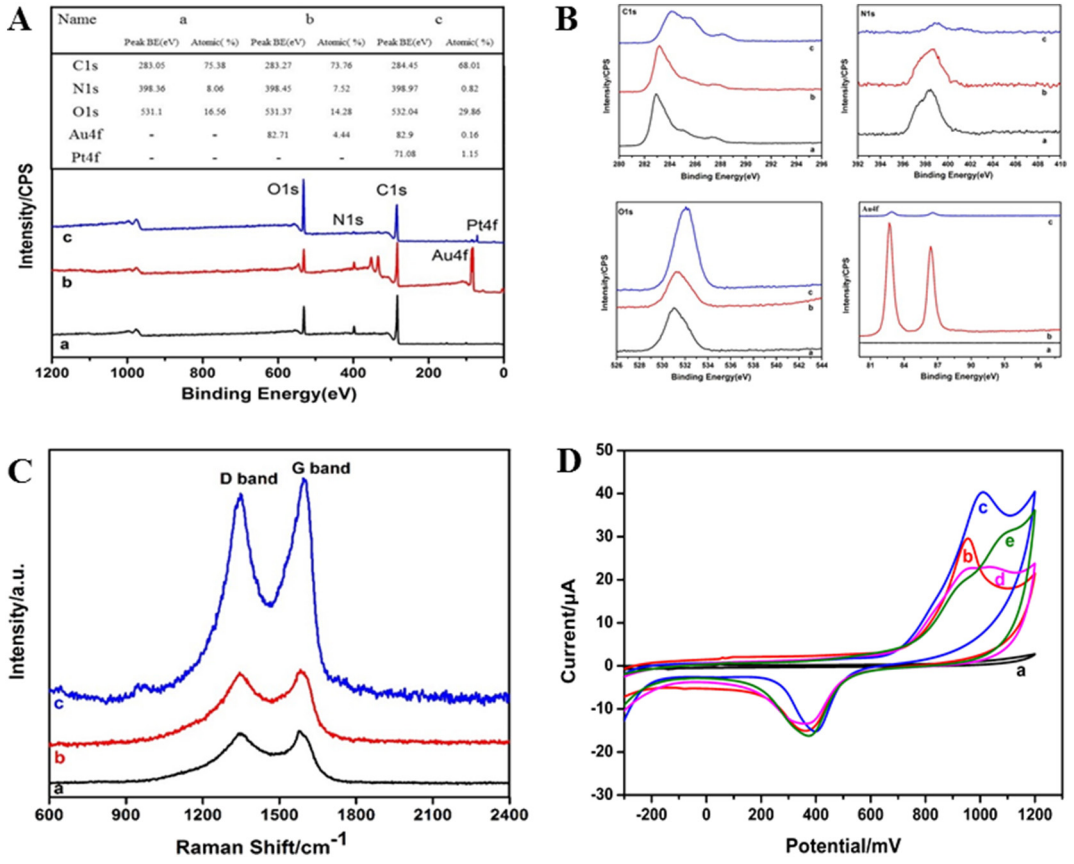

Fig. 4. XPS spectra of the surface of SPCE in different stages: (A) Full spectra; (B) XPS spectra of C1s, N1 s, O1s and Au4f for bare SPCE (a); Au NPs/SPCE (b); RGO-PT-Pt/Au NPs/SPCE (c); (C) Raman spectra for bare SPCE (a), Au NPs/SPCE (b), RGO-PT-Pt/Au NPs/SPCE (c); (D) Cyclic voltammetry response for bare SPCE (a), Au NPs/SPCE (b), RGO/Au NPs/SPCE (c), RGO-PT/Au NPs/SPCE (d),RGO-PT-Pt/Au NPs/SPCE (e) in the presence of 0.1 mM H_2O_2 in PBS from −0.7 to 0.8 V with 100 m V/s scanning rate.

distinguishing between sp^2 and sp^3 hybridization in carbonaceous materials. Fig. 4C depicted the Raman spectroscopy for different stages of SPCE modification. Seen from the Fig.4C, the two main characteristic Raman bands can be seen obviously at 1347.939 cm^{-1} (D-band) and 1592.854 cm^{-1} (G-band). The intensity of D-band and G-band of RGO-PT-Pt/Au NPs/SPCE was higher than those of bare SPCE and Au NPs/SPCE. By calculation, the value of I_D/I_G for RGO-PT-Pt/Au NPs/SPCE was 0.925, while the I_D/I_G for Au NPs/SPCE was 0.974 and 0.957 for bare SPCE. This is may be the fact that RGO-PT-Pt has been successfully immobilized on the electrode surface and changed the intensity of D-band and G-band, specifying the decreased structural disorders of the surface of SPCE.

3.7. RGO-PT-Pt non-enzymatic biosensor for the detection of H_2O_2

Fig.4D showed CV response of the constructed non-enzymatic biosensor for the detection of H_2O_2. A reduction peak of H_2O_2 emerged in the presence of 0.1 mM H_2O_2 in PBS (curve c → e) and the RGO-PT-Pt/Au NPs/SPCE (curve e) had the highest reduction peak current of H_2O_2. As a control, a negligible reduction peak of H_2O_2 can be obtained on bare SPCE (curve a). These results indicated that the construction of the non-enzymatic was relatively successful and the experimental results are consistent with the report [2]. This is may be the fact that the RGO-PT-Pt nanocomposite revealed better catalytic ability to H_2O_2 via synergistic effect. The synergistic effect of PT, RGO and Pt NPs provided excellent catalytic ability for disintegration of the H_2O_2 and electron conductivity, which can efficiently amplifying the current signal for H_2O_2 detection.

3.8. Optimization of experimental conditions for the RGO-PT-Pt non-enzymatic biosensor for detection H_2O_2

To achieve the best performance for the RGO-PT-Pt non-enzymatic biosensor, the experimental conditions for H_2O_2 detection was optimized by varying different the layers of RGO-PT-Pt nanocomposite, the concentrations of the RGO-PT-Pt nanocomposite, the pH of the buffer solution, and the detection potential. Fig. 5A showed the effect of different layers of RGO-PT-Pt nanocomposites on the current response of the RGO-PT-Pt non-enzymatic biosensor. Seen from Fig. 5A, the current response of the biosensor gradually increased with the increase of the amount of RGO-PT-Pt nanocomposite and reached the highest peak with three layers. Then the current response began to decline gradually as the increasing of the layers of RGO-PT-Pt nanocomposite. Thus, three layers of RGO-PT-Pt film were chosen for further experiments.

Fig. 5B showed the change in H_2O_2 current response in different concentrations of the RGO-PT-Pt nanocomposite. As can be seen from Fig. 5B, the current response increased as the concentration increased. When the concentration of the RGO-PT-Pt nanocomposite was 1.0 mg/mL, the current increase gradually tended to be flat, Therefore, the concentration of 1.0 mg/mL for the RGO-PT-Pt nanocomposite was selected for subsequent experiments.

Fig. 5C indicated the change of the current response value of H_2O_2 in PBS with different pH value (6.0–8.0). It can be seen from Fig. 5C that the current response increased first and then decreased with increase of pH value. The amperometric response was the highest when the pH was 7.4, indicated that the biosensor was more active at this pH value. Thus, pH 7.4 was chosen as the optimum working pH for the reaction medium, which was close to the normal pH of the human

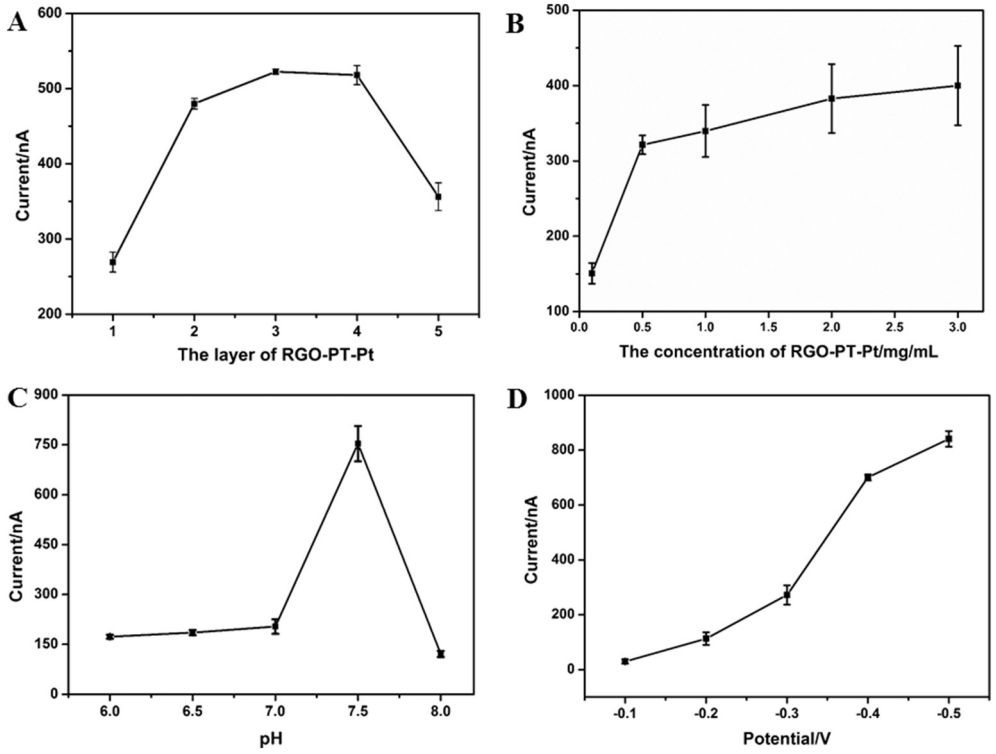

Fig. 5. (A) Effect of layer number of RGO-PT-Pt composite on current response; (B) Effect of the concentration of RGO-PT-Pt composite on current response; (C) Effect of pH on current response; (D) Effect of the potentials on current response. Error bars indicated the relative standard deviation of three repetitive experiments.

environment.

Fig. 5D represented the results of the relation between the current response and potentials. Seen from Fig. 5D, the amperometric response was gradually intensified with the detection potential changed from −0.1 to −0.5 V. At potentials more negative than −0.1 V, H_2O_2 is electrochemically reduced in neutral solutions, and the current signal increases accordingly with the applied potential negatively shifting to −0.5 V. With consideration of the interferences from other physiological materials, the applied potential of −0.4 V is regarded as an appropriate compromise between sensitivity and selectivity [2, 41].

3.9. Performance of the RGO-PT-Pt non-enzymatic biosensor towards H_2O_2

Herein we use the RGO-PT-Pt non-enzymatic biosensor to facilitate the reduction of H_2O_2 and measure the reduction current at a certain potential using the current-time technique. Under the optimized conditions, the developed RGO-PT-Pt non-enzymatic biosensor was used and the current response was recorded for the successive addition of H_2O_2 with different concentrations in PBS (Fig. 6A). Seen from Fig. 6A, the current response increased with the increasing H_2O_2 concentration. And the RGO-PT-Pt/Au NPs/SPCE responded very rapidly to the addition of H_2O_2, producing steady-state signals within 3 s. Fig. 6B was the calibration curve of the RGO-PT-Pt non-enzymatic biosensor for the detection of different concentrations of H_2O_2. As shown in Fig. 6B, the concentration of H_2O_2 was in satisfactory linear relationship with the response current at the range of 1.0–100.0 μM. The linear equation was $I_{(nA)} = 43.55C_{(\mu M)} + 207.81$ with a correlation coefficient of 0.9931. The sensitivity, expressed as the slope of the calibration straight-line section, was calculated from the plot of Fig. 6B by means of linear regression. With the help of a linear regression of these values, the sensitivity was calculated to be 0.780 μA μM^{-1} cm^{-2}. The limits of detection (LOD), defined as $C_{LOD} = 3S_b/b$, where S_b was the standard deviation of 6 replicate blank signals and b was the slope of the linear section of calibration curve, had been calculated to be 0.26 μM at the signal-to-noise ratio of 3.

Furthermore, the analytical performance of the proposed biosensor was compared with other non-enzymatic H_2O_2 biosensors, as summarized in Table 1. Seen from Table 1, the performance of the RGO-PT-Pt non-enzymatic biosensor was better than previously reported sensors. These excellent performances of the RGO-PT-Pt non-enzymatic biosensor may be attributed to synergistic effect of the high electrocatalytic efficiency of Pt NPs, high electronic conductivity of RGO and the adsorption ability of PT on metal ions. In addition, it was further demonstrated that RGO-PT-Pt is a promising nanomaterial for the modified electrodes for detection of H_2O_2.

3.10. Specificity, reproducibility and stability of the RGO-PT-Pt non-enzymatic biosensor

The specificity of the RGO-PT-Pt non-enzymatic biosensor was investigated by comparing the amperometric responses of successive addition of 0.1 mM H2O2, 0.1 mM AA, 0.1 mM UA, 0.1 mM DA, 0.1 mM DOPAC and 0.1 mM H_2O_2 in 10 mL of PBS at the applied potential of −0.4 V. As shown in Fig. 6C, the response current increased obviously after addition of H_2O_2, and no obvious changed after the addition of AA, UA, DA, DOPAC, respectively, while the current obviously increased again after $H_2O_2{}^+$was secondly added. These results showed that the responses caused by AA, UA, DA and DOPAC could be negligible, which indicated that the RGO-PT-Pt non-enzymatic biosensor has a good selectivity and can be used for the detection of H_2O_2 without any effect caused by possible interferents.

The reproducibility was assessed by detecting the responses to 10 μM H_2O_2 at five electrodes independently. The relative standard deviation (RSD) was calculated to 4.0%. Furthermore, the stability of the RGO-PT-Pt non-enzymatic biosensor was evaluated by placing the prepared RGO-PT-Pt non-enzymatic biosensor in a humid environment at 4 °C when the sensors were out of use, and measuring its response current to 10 μM H_2O_2 solution every 2 days. A 4.23% decrease in the current response was observed after 4 days and 8.85% decrease after 8 days. Eventually, the current response maintained its initial current

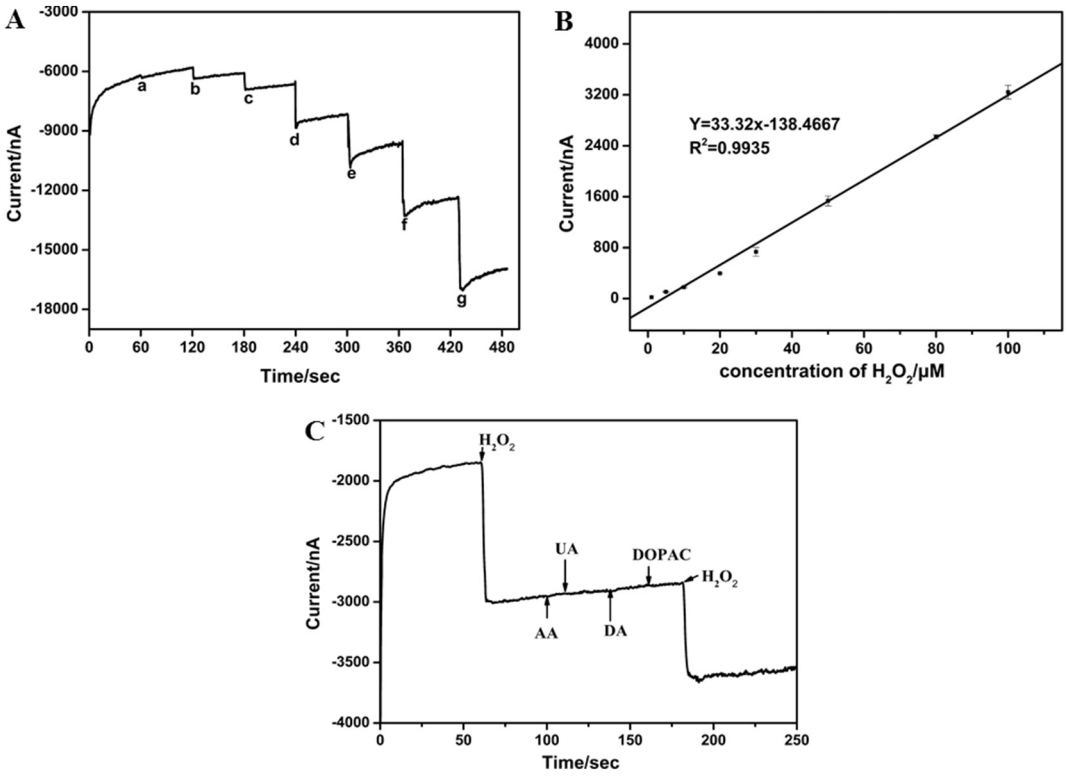

Fig. 6. (A) Current-time curves of different concentrations of H_2O_2 including 1, 5, 10, 30, 50, 80, 100 μM (a–g); (B) Calibration curve of the non-enzymatic biosensor sensor for the detection of different concentrations of H_2O_2. The current signal was obtained by i-t technique which was carried out in PBS at −0.4 V with agitation rate about 100 rpm. And the error bars represent the relative standard deviation (n = 3 electrodes); (C) Current-time curve of RGO-PT-Pt/Au NPs/SPCE with successive additions of 100 μM H_2O_2, 100 μM AA, 100 μM UA, 100 μM DA, 100 μM DOPAC and 100 μM H_2O_2 at RGO-PT-Pt/Au NPs/SPCE electrode at the potential of −0.40 V in PBS with stirred 100 rpm rate.

Table 1
Comparison of the electroanalytical parameters for a variety of electrodes modified with Pt NPs for the detection of H_2O_2.

Electrode	Applied potential (V)	Electrolyte pH	LOD (μM)	References
Pt NPs/SPCEs	0.2–0.7	PBS (7.4)	16	[38]
Pt/Cu/GCE	0.3	PBS (7.4)	12.2	[39]
Au-Pt BM-NPs/SPCEs	0.4	PBS (7.4)	10	[40]
MWCNTC/Pt NPs/ SPCEs	−0.4	PBS (6.9)	1.23	[41]
Pt NPs-CNF PDDA /SPCEs	0.5	PBS (7.0)	2.4	[42]
Pt-polypyrrole/GCE	−0.1	PBS (7.0)	1.2	[43]
RGO/CS/Fc/Pt/GE	−0.05	PBS (7.0)	0.02	[44]
Pt NPs/SPCEs	0.7	PBS (7.0)	1.9	[12]
RGO-PT-Pt NPs/ SPCEs	−0.4	PBS (7.4)	0.26	This work

response of 89.00% after 20 days. Thus, these results indicated the prepared sensor exhibited an acceptable reproducibility and stability.

3.11. Real human serum sample analysis

In order to verify the practical application of the prepared sensor, the feasibility of the proposed H_2O_2 detection method in real human serum samples was evaluated using the standard addition method. The experimental results are shown in Table 2. From Table 2, it can be seen that the recovery rate is between 98.38% and 108.90%. The satisfying results demonstrated that the biosensor had a great potential for practical application.

Table 2
Determination of H_2O_2 in human serum samples with RGO-PT-Pt non-enzymatic biosensor.

H_2O_2 added (μM)	Response current (nA)	Concentration Found (μM)	Recovery (%)
15	320	14.757 ± 1.007	98.38
	380		
	360		
40	1280	43.571 ± 3.901	108.90%
	1210		
	1440		
60	1960	57.977 ± 5.00	96.63%
	1540		
	1880		

4. Conclusions

In summary, a facile and effective non-enzymatic electrochemical biosensor for H_2O_2 detection was constructed based on RGO-PT-Pt nanocomposite. The RGO-PT-Pt nanocomposite was prepared by facile reduction method with AA as reducing agent. Taking advantage of high electro-catalytic efficiency of Pt nanoparticles, high electronic conductivity and large surface area of RGO, and significant adsorption ability of PT on metal ions and its prevention of agglomeration to promote RGO dispersion, the RGO-PT-Pt nanocomposite revealed better catalytic ability towards H_2O_2 via a synergistic effect. Under the optimal conditions, the prepared RGO-PT-Pt non-enzymatic biosensor responded very rapidly towards H_2O_2, producing steady-state signals within 3 s. The linear relationship between the amperometric current response and the H_2O_2 concentration was very well over the range from 1.0 μM to 100 μM with a readily achievable detection limit of 0.26 μM (S/N = 3). In addition, the fabricated sensor demonstrated the practical

applicability in human serum samples with the appreciable recovery and also exhibited the excellent performances in terms of selectivity, reliability, reproducibility and stability. The RGO-PT-Pt non-enzymatic biosensor can be very useful for detection of H_2O_2 and offer great potential in providing a sensitive and potent method for detection of H_2O_2 in clinical diagnostics.

Acknowledgments

This work was supported by the National Nature Science Foundation of China (Nos. 81460451, 81760534 and 81430055), the Innovation Project of GUET Graduate Education (Nos. YCSW2017146 and 2017YJCX95), and the Nature Science Foundation of Guangxi Province of China (Nos. 2015GXNSFDA139025, 2016GXNSFAA380011 and 2016GXNSFAA380080).

References

[1] Y. Sun, M. Luo, X. Meng, J. Xiang, L. Wang, Q. Ren, S. Guo, Graphene/intermetallic PtPb nanoplates composites for boosting electrochemical detection of H_2O_2 released from cells, Anal. Chem. 89 (2017) 3761–3767.
[2] G. Gnana Kumar, K. Justice Babu, K.S. Nahm, Y.J. Hwang, A facile one-pot green synthesis of reduced graphene oxide and its composites for non-enzymatic hydrogen peroxide sensor applications, RSC Adv. 4 (2014) 7944–7951.
[3] A.A. Ensafi, F. Rezaloo, B. Rezaei, Electrochemical sensor based on porous silicon/silver nanocomposite for the determination of hydrogen peroxide, Sensors Actuators B Chem. 231 (2016) 239–244.
[4] X. Zhu, X. Niu, H. Zhao, M. Lan, Doping ionic liquid into Prussian blue-multiwalled carbon nanotubes modified screen-printed electrode to enhance the nonenzymatic H_2O_2 sensing performance, Sensors Actuators B Chem. 195 (2014) 274–280.
[5] A. Lascu, A. Palade, G. Fagadar-Cosma, I. Creanga, C. Ianasi, I. Sebarchievici, M. Birdeanu, E. Fagadar-Cosma, Mesoporous manganese–porphyrin–silica hybrid nanomaterial sensitive to H_2O_2 fluorescent detection, Mater. Res. Bull. 74 (2016) 325–332.
[6] W. Xue, X. Bo, M. Zhou, L. Guo, Enzymeless electrochemical detection of hydrogen peroxide at Pd nanoparticles/porous graphene, J. Electroanal. Chem. 781 (2016) 204–211.
[7] N.V. Klassen, D. Marchington, H.C.E. McGowan, H_2O_2 determination by the I_3-method and by $KMnO_4$ titration, Anal. Chem. 66 (1994) 2921–2925.
[8] L.F. Lu, Y.Y. Li, M. Zhang, G. Shi, Visual fluorescence detection of H_2O_2 and glucose based on “molecular beacon”-hosted Hochest dyes, Analyst 140 (2015) 3642–3647.
[9] K. Kikuchi, T. Nagano, H. Hayakawa, Y. Hirata, M. Hirobe, Real time measurement of nitric oxide produced ex vivo by luminol-H_2O_2 chemiluminescence method, J. Biol. Chem. 5 (1993) 23106–23110.
[10] X. Zhang, X. Bi, W. Di, W. Qin, A simple and sensitive $Ce(OH)CO_3/H_2O_2$/TMB reaction system for colorimetric determination of H_2O_2 and glucose, Sensors Actuators B Chem. 231 (2016) 714–722.
[11] M. Yang, D.S. Kim, T.J. Lee, S.J. Lee, K.G. Lee, B.G. Choi, Polyoxometalate-grafted graphene nanohybrid for electrochemical detection of hydrogen peroxide and glucose, J. Colloid Interface Sci. 468 (2016) 51–56.
[12] J. Agrisuelas, M.I. González-Sánchez, E. Valero, Hydrogen peroxide sensor based on in situ grown Pt nanoparticles from waste screen-printed electrodes, Sensors Actuators B Chem. 249 (2017) 499–505.
[13] C. Zhao, H. Zhang, J. Zheng, A non-enzymatic electrochemical hydrogen peroxide sensor based on Ag decorated boehmite nanotubes/reduced graphene oxide nanocomposites, J. Electroanal. Chem. 784 (2017) 55–61.
[14] H. Hao, Q. Sheng, J. Zheng, One-step synthesis of Ag@SiO_2@Ag nanomaterial and its application as hydrogen peroxide sensor, Colloids Surf. A Physicochem. Eng. Asp. 518 (2017) 124–129.
[15] Y. Huang, L. Cui, Y. Xue, S. Zhang, N. Zhu, J. Liang, G. Li, Ultrasensitive cholesterol biosensor based on enzymatic silver deposition on gold nanoparticles modified screen-printed carbon electrode, Mater. Sci. Eng. C 77 (2017) 1–8.
[16] Y. Wang, Z. Wang, Y. Rui, M. Li, Horseradish peroxidase immobilization on carbon nanodots/CoFe layered double hydroxides: direct electrochemistry and hydrogen peroxide sensing, Biosens. Bioelectron. 64 (2015) 57–62.
[17] Z. Yang, X. Zheng, J. Zheng, Non-enzymatic sensor based on a glassy carbon electrode modified with Ag nanoparticles/polyaniline/halloysite nanotube nanocomposites for hydrogen peroxide sensing, RSC Adv. 6 (2016) 58329–58335.
[18] T.D. Thanh, J. Balamurugan, S.H. Lee, N.H. Kim, J.H. Lee, Novel porous gold-palladium nanoalloy network-supported graphene as an advanced catalyst for non-enzymatic hydrogen peroxide sensing, Biosens. Bioelectron. 85 (2016) 669–678.
[19] J.G. Roberts, M.A. Voinov, A.C. Schmidt, T.I. Smirnova, L.A. Sombers, The hydroxyl radical is a critical intermediate in the voltammetric detection of hydrogen peroxide, J. Am. Chem. Soc. 138 (2016) 2516–2519.
[20] Y. Zhang, X. Bai, X. Wang, K.K. Shiu, Y. Zhu, H. Jiang, Highly sensitive graphene-Pt nanocomposites amperometric biosensor and its application in living cell H_2O_2 detection, Anal. Chem. 86 (2014) 9459–9465.
[21] F. Lorestani, Z. Shahnavaz, P. Mn, Y. Alias, N.S.A. Manan, One-step hydrothermal green synthesis of silver nanoparticle-carbon nanotube reduced-graphene oxide composite and its application as hydrogen peroxide sensor, Sensors Actuators B Chem. 208 (2015) 389–398.
[22] J. Salamon, Y. Sathishkumar, K. Ramachandran, Y.S. Lee, D.J. Yoo, A.R. Kim, G. Gnana Kumar, One-pot synthesis of magnetite nanorods/graphene composites and its catalytic activity toward electrochemical detection of dopamine, Biosens. Bioelectron. 64 (2015) 269–276.
[23] G. Gnana Kumar, G. Amala, S.M. Gowtham, Recent advancements, key challenges and solutions in non-enzymatic electrochemical glucose sensors based on graphene platforms, RSC Adv. 7 (2017) 36949–36976.
[24] H. Yin, Y. Zhou, Q. Ma, S. Ai, P. Ju, L. Zhu, L. Lu, Electrochemical oxidation behavior of guanine and adenine on graphene–Nafion composite film modified glassy carbon electrode and the simultaneous determination, Process Biochem. 45 (2010) 1707–1712.
[25] K. Justice Babu, S. Sheet, Y.S. Lee, G. Gnana Kumar, Three-dimensional dendrite Cu–Co/reduced graphene oxide architectures on a disposable pencil graphite electrode as an electrochemical sensor for nonenzymatic glucose detection, ACS Sustain. Chem. Eng. 6 (2018) 1909–1918.
[26] Z. Zhou, Y. Huang, J. Liang, M. Ou, J. Chen, G. Li, Extraction, purification and anti-radiation activity of persimmon tannin from diospyros kaki L.f, J. Environ. Radioact. 162–163 (2016) 182–188.
[27] Z. Zhou, F. Liu, Y. Huang, Z. Wang, G. Li, Biosorption of palladium(II) from aqueous solution by grafting chitosan on persimmon tannin extract, Int. J. Biol. Macromol. 77 (2015) 336–343.
[28] Z. Wang, X. Li, H. Liang, J. Ning, Z. Zhou, G. Li, Equilibrium, kinetics and mechanism of Au^{3+}, Pd^{2+} and Ag^{+} ions adsorption from aqueous solutions by graphene oxide functionalized persimmon tannin, Mater. Sci. Eng. C 79 (2017) 227–236.
[29] Q. Yi, R. Fan, F. Xie, H. Min, Q. Zhang, Z. Luo, Selective recovery of Au(III) and Pd (II) from waste pcbs using ethylenediamine modified persimmon tannin adsorbent, Procedia Environ Sci 31 (2016) 185–194.
[30] M. Gurung, B.B. Adhikari, S. Alam, H. Kawakita, K. Ohto, K. Inoue, Persimmon tannin-based new sorption material for resource recycling and recovery of precious metals, Chem. Eng. J. 228 (2013) 405–414.
[31] Y. Zheng, A. Wang, W. Cai, Z. Wang, F. Peng, Z. Liu, L. Fu, Hydrothermal preparation of reduced graphene oxide-silver nanocomposite using *Plectranthus amboinicus* leaf extract and its electrochemical performance, Enzym. Microb. Technol. 95 (2016) 112–117.
[32] P. Vennila, D.J. Yoo, A.R. Kim, G.G. Kumar, Ni-Co/Fe_3O_4 flower-like nanocomposite for the highly sensitive and selective enzyme free glucose sensor applications, J. Alloys Compd. 703 (2017) 633–642.
[33] K. Ramachandran, T. Raj Kumar, K.J. Babu, G. Gnana Kumar, Ni-Co bimetal nanowires filled multiwalled carbon nanotubes for the highly sensitive and selective non-enzymatic glucose sensor applications, Sci. Rep. 6 (2016) 36583–36589.
[34] K.J. Babu, N. Senthilkumar, A.R. Kim, G.G. Kumar, Freestanding and binder free PVdF-HFP/Ni-Co nanofiber membrane as a versatile platform for the electrocatalytic oxidation and non-enzymatic detection of urea, Sensors Actuators B Chem. 24 (2017) 541–551.
[35] N. Senthilkumar, G. Gnana Kumar, A. Manthiram, 3D hierarchical core-shell nanostructured arrays on carbon fibers as catalysts for direct urea fuel cells, Adv. Energy Mater. 8 (2018) 1702201–1702211.
[36] Y. Fang, D. Zhang, X. Qin, Z. Miao, S. Takahashi, J.-i. Anzai, Q. Chen, A non-enzymatic hydrogen peroxide sensor based on poly(vinyl alcohol)–multiwalled carbon nanotubes–platinum nanoparticles hybrids modified glassy carbon electrode, Electrochim. Acta 70 (2012) 266–271.
[37] M. Yang, Y. Yang, Y. Liu, G. Shen, R. Yu, Platinum nanoparticles-doped sol-gel/carbon nanotubes composite electrochemical sensors and biosensors, Biosens. Bioelectron. 21 (2006) 1125–1131.
[38] M. Chikae, K. Idegami, K. Kerman, N. Nagatani, M. Ishikawa, Y. Takamura, E. Tamiya, Direct fabrication of catalytic metal nanoparticles onto the surface of a screen-printed carbon electrode, Electrochem. Commun. 8 (2006) 1375–1380.
[39] M. Janyasupaba, W.L. Chen, Y. Zhangc, W.W. Kuan, C.C. Liu, Bimetallic Pt–M (M = Cu, Ni, Pd, and Rh) nanoporous for H_2O_2 based amperometric biosensors, Sensors Actuators B Chem. 179 (2013) 209–214.
[40] S. Upadhyay, M.K. Sharma, G. Rama Rao, B.K. Bhattacharya, V.K. Rao, R. Vijayaraghavan, Application of bimetallic nanoparticles modified screen printed electrode for the detection of organophosphate compounds using an enzyme inhibition approach, Anal. Methods 3 (2011) 2246–2253.
[41] X. Niu, H. Zhao, C. Chen, M. Lan, Platinum nanoparticle-decorated carbon nanotube clusters on screen-printed gold nanofilm electrode for enhanced electrocatalytic reduction of hydrogen peroxide, Electrochim. Acta 65 (2012) 97–103.
[42] P.J. Lamas-Ardisana, O.A. Loaiza, L. Anorga, E. Jubete, M. Borghei, V. Ruiz, E. Ochoteco, G. Cabanero, H.J. Grande, Disposable amperometric biosensor based on lactate oxidase immobilised on platinum nanoparticle-decorated carbon nanofiber and poly(diallyldimethylammonium chloride) films, Biosens. Bioelectron. 56 (2014) 345–351.
[43] X.J. Bian, X.F. Lu, E. Jin, L.R. Kong, C. Wang Wj Zhang, Fabrication of Pt/polypyrrole hybrid hollow microspheres and their application in electrochemical biosensing towards hydrogen peroxide, Talanta 81 (2010) 813–818.
[44] Z. Bai, G. Li, J. Liang, J. Su, Y. Zhang, H. Chen, Y. Huang, W. Sui, Y. Zhao, Non-enzymatic electrochemical biosensor based on Pt NPs/RGO-CS-Fc nano-hybrids for the detection of hydrogen peroxide in living cells, Biosens. Bioelectron. 82 (2016) 185–194.